Lamin B1 controls oxidative stress responses via Oct-1

Ashraf N. Malhas,[1] Chiu Fan Lee,[2] and David J. Vaux[1]

[1]Sir William Dunn School of Pathology and [2]Clarendon Laboratory, Department of Physics, University of Oxford, Oxford OX1 2JD, England, UK

Interaction of lamins with chromatin and transcription factors regulate transcription. Oct-1 has previously been shown to colocalize partly with B-type lamins and is essential for transcriptional regulation of oxidative stress response genes. Using sequential extraction, co-immunoprecipitation (IP), fluorescence loss in photobleaching, and fluorescence resonance energy transfer, we confirm Oct-1–lamin B1 association at the nuclear periphery and show that this association is lost in *Lmnb1*$^{\Delta/\Delta}$ cells. We show that several Oct-1–dependent genes, including a subset involved in oxidative stress response, are dysregulated in *Lmnb1*$^{\Delta/\Delta}$ cells. Electrophoretic mobility shift assay and chromatin IP reveal that Oct-1 binds to the putative octamer-binding sequences of the dysregulated genes and that this activity is increased in cells lacking functional lamin B1. Like *Oct1*$^{-/-}$ cells, *Lmnb1*$^{\Delta/\Delta}$ cells have elevated levels of reactive oxygen species and are more susceptible to oxidative stress. Sequestration of Oct-1 at the nuclear periphery by lamin B1 may be a mechanism by which the nuclear envelope can regulate gene expression and contribute to the cellular response to stress, development, and aging.

Introduction

The nuclear lamina underlies the inner nuclear membrane and is therefore an integral part of the nuclear envelope. The major components of the lamina are nuclear lamins, intermediate filament proteins encoded by three genes in humans, *LMNA*, *LMNB1*, and *LMNB2*. The *LMNA* gene encodes A-type lamins, whereas the B-type lamins, lamin B1 and lamins B2 and B3, are encoded by the *LMNB1* and *LMNB2* genes, respectively. A-type lamins are developmentally regulated and are expressed in differentiated cells, whereas at least one B-type lamin is expressed in all vertebrate cells (for review see Goldman et al., 2002). The nuclear lamina provides structural support and is involved in anchoring chromatin to the nuclear envelope in DNA replication and repair and in the control of gene expression (Worman and Courvalin, 2005; Tang et al., 2008). It is through these mechanisms that nuclear shape, and thus the nuclear lamina, is associated with the normal aging process as well as with premature aging disorders (Haithcock et al., 2005; Lans and Hoeijmakers, 2006; Scaffidi and Misteli, 2006).

We and others have previously reported that chromatin interactions with the nuclear envelope play important roles in the control of gene expression (Hewitt et al., 2004; Zink et al., 2004; Chuang et al., 2006; Malhas et al., 2007; Guelen et al., 2008). An alternative mechanism by which the nuclear envelope can regulate gene expression is by associating with specific transcription factors (Heessen and Fornerod, 2007), such as AP-1, sterol regulatory element-binding protein, MOK2, and the octamer transcription factor 1 (Oct-1), and modulating their activities (Imai et al., 1997; Dreuillet et al., 2002, 2008; Lloyd et al., 2002; Capanni et al., 2005; Ivorra et al., 2006). Oct-1 is a ubiquitous transcription factor known to have both activating and silencing activities. Two lines of evidence suggest a role for the nuclear lamina in associating with and regulating the activity of Oct-1. First, Oct-1 has been shown to be present in an insoluble nuclear fraction (Kim et al., 1996), suggesting that it may be associated with the nuclear lamina. Second, Imai et al. (1997) have shown that the dissociation of Oct-1 from the nuclear periphery is accompanied by the upregulation of the interstitial collagenase gene and is associated with cellular aging.

Correspondence to David J. Vaux: david.vaux@path.ox.ac.uk

Abbreviations used in this paper: ChIP, chromatin IP; EMSA, electrophoretic mobility shift assay; FLIP, fluorescence loss in photobleaching; FRET, fluorescence resonance energy transfer; IP, immunoprecipitation; MAPPER, multigenome analysis of positions and patterns of elements of regulation; qRT-PCR, quantitative real-time PCR; ROI, region of interest; ROS, reactive oxygen species; WT, wild type.

© 2009 Malhas et al. This article is distributed under the terms of an Attribution–Noncommercial–Share Alike–No Mirror Sites license for the first six months after the publication date (see http://www.jcb.org/misc/terms.shtml). After six months it is available under a Creative Commons License (Attribution–Noncommercial–Share Alike 3.0 Unported license, as described at http://creativecommons.org/licenses/by-nc-sa/3.0/).

The Rockefeller University Press $30.00
J. Cell Biol. Vol. 184 No. 1 45–55
www.jcb.org/cgi/doi/10.1083/jcb.200804155

THE JOURNAL OF CELL BIOLOGY

Downloaded from http://rupress.org/jcb/article-pdf/184/1/45/1555786/jcb_200804155.pdf by guest on 08 February 2026

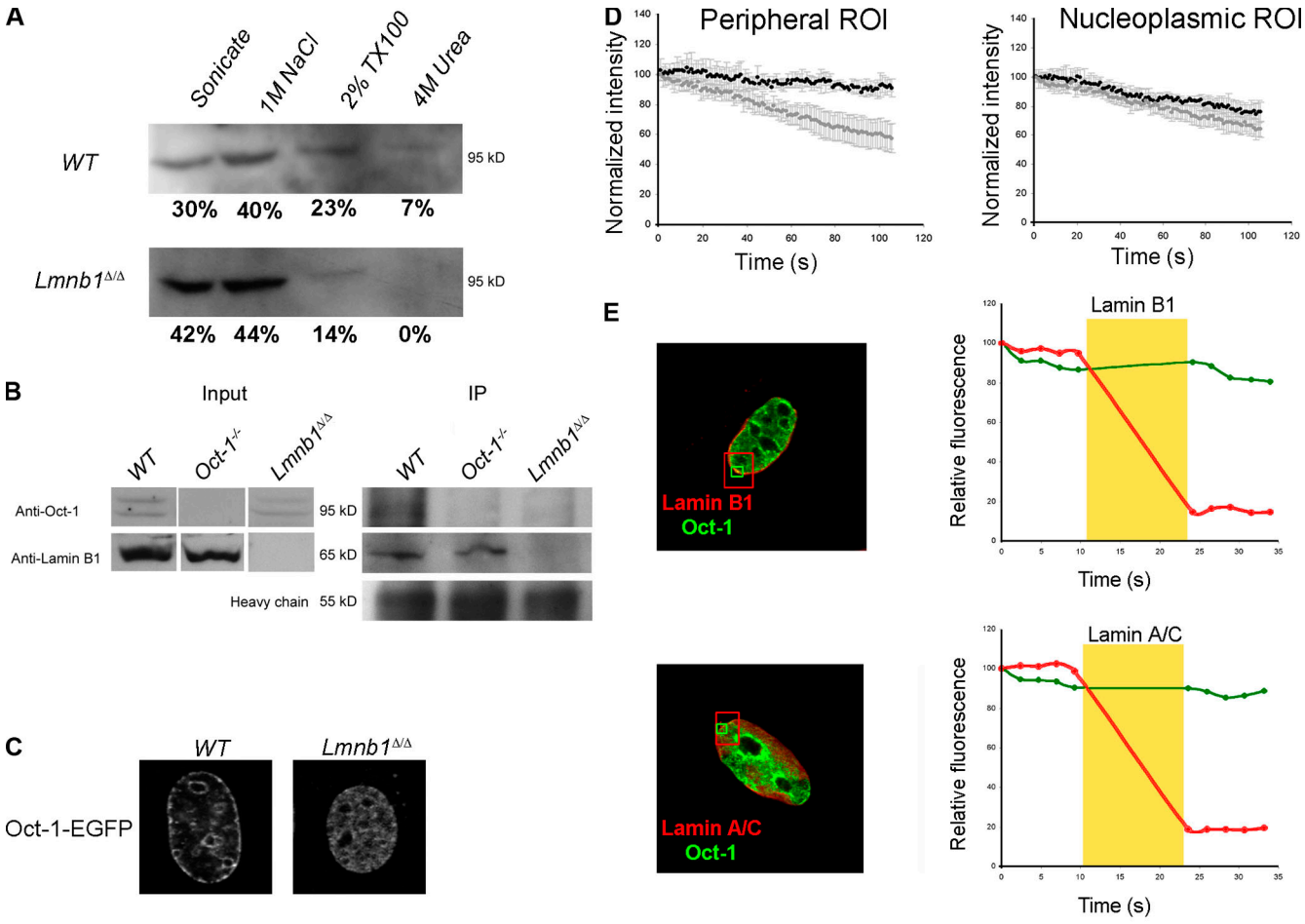

Figure 1. **Oct-1 is tightly associated with lamin B1.** (A) Nuclei from WT and *Lmnb1*$^{\Delta/\Delta}$ cells were subjected to sequential extraction and analyzed by Western blotting. Numbers represent percentages of Oct-1 signal in each fraction from one representative experiment. (B) Oct-1 is coimmunoprecipitated with lamin B1 from lysates of WT but not *Oct1*$^{-/-}$ or *Lmnb1*$^{\Delta/\Delta}$ cells. The left panels show immunoblots of the input sample, and the right panels show immunoblots of the immunoprecipitates. A control staining of the immunoprecipitates with anti–goat heavy chain confirms equivalent precipitation efficiency in each sample. (C) Oct-1–EGFP shows nuclear peripheral association in living WTs but not in *Lmnb1*$^{\Delta/\Delta}$ cells. (D) FLIP in WT and *Lmnb1*$^{\Delta/\Delta}$ cells expressing Oct-1–EGFP. (left) A nuclear peripheral ROI outside the photobleached area was used to measure fluorescence loss after photobleaching (mean values ± SD shown; $n = 10$). These results indicate that Oct-1–EGFP is more tightly associated with the peripheral nuclear lamina containing full-length lamin B1. (right) Quantitative FLIP of a nucleoplasmic ROI shows that there is no significant difference in stability of nucleoplasmic Oct-1–EGFP expressed in WT or *Lmnb1*$^{\Delta/\Delta}$ cells. (E) Oct-1 is in tight association with lamin B1 but not lamin A/C. FRET was performed as described in Materials and methods. The red boxes (images) and lines (plots) represent the ROI that was selected for acceptor photobleaching using the 543-nm laser, whereas the green boxes and lines represent an ROI selected within the photobleached regions for analysis of FRET. The shaded areas in the plots show the time of bleaching. Note the increase in donor (green) fluorescence after bleaching lamin B1 (top) but not lamin A/C (bottom), indicating that the nuclear lamina component in association with Oct-1 is indeed lamin B1 and not lamin A/C. A representative image is shown (5% FRET efficiency for lamin B1), but mean FRET efficiency values (4.63 ± 1.4% SD and 0 ± 0.75% SD for lamin B1 and lamin A/C, respectively) from 20 nuclei in three independent experiments show a significant difference using a Student's *t* test ($P < 0.01$).

More recently, Tantin et al. (2005) have shown that Oct-1 regulates genes that are essential for the cellular response to stress and that Oct-1–deficient mouse fibroblasts harbored elevated levels of reactive oxygen species (ROS) and were more susceptible to oxidative stress. Given the link between aging and ROS (for review see Finkel and Holbrook, 2000) and that alterations to the nuclear envelope occur during aging, we hypothesized that the nuclear lamina and Oct-1 might have a cooperative role in controlling the expression of genes that are associated with aging and response to oxidative stress. To examine this hypothesis, we first confirmed that lamin B1 is associated with Oct-1 in normal mouse fibroblasts but not in cells lacking normal, full-length lamin B1 (*Lmnb1*$^{\Delta/\Delta}$ cells). We also found that, like Oct-1–deficient fibroblasts, *Lmnb1*$^{\Delta/\Delta}$ cells have elevated ROS levels and that they are more susceptible to oxidative stress than normal mouse fibroblasts as a result of the same gene expression abnormalities. We demonstrate that the release of Oct-1 in the *Lmnb1*$^{\Delta/\Delta}$ cells results in increased occupancy of its binding sites in target genes that are dysregulated in Oct-1– and lamin B1–deficient cells. Collectively, our results provide evidence that lamin B1 at the nuclear lamina directly sequesters Oct-1 and as a result can regulate the expression of genes involved in various processes, including aging and response to oxidative stress.

Results

Oct-1–lamin B1 interactions

Western blotting detection of Oct-1 confirmed the presence of two isoforms of the protein at comparable levels in wild-type

Downloaded from http://rupress.org/jcb/article-pdf/184/1/45/1555786/jcb_200804155.pdf by guest on 08 February 2026

(WT) mouse embryonic fibroblasts and *Lmnb1*$^{\Delta/\Delta}$ cells that lack the C-terminal 273 amino acids of lamin B1 (Vergnes et al., 2004). Using a previously described nuclear envelope subfractionation protocol involving differential extraction (Maske et al., 2003), we found that in WT cells, Oct-1 is detected in all fractions of increasing extraction stringency, including the 4-M urea fraction. However, in *Lmnb1*$^{\Delta/\Delta}$ cells, more Oct-1 is released in the earlier fractions, and no Oct-1 is detected in the 4 M urea fraction (Fig. 1 A). This profile of extraction is consistent with tight association with the nuclear lamina because in WT cells, this pool contains >40% of the full-length lamin B1 in the nucleus (Maske et al., 2003). Immunoprecipitating lysates from WT cells with an anti–lamin B1 antibody resulted in coimmunoprecipitating Oct-1 (Fig. 1 B). Oct-1 was not coimmunoprecipitated with lamin B1 in lysates of *Oct1*$^{-/-}$ cells despite the successful precipitation of lamin B1. The anti–lamin B1 antibody used in immunoprecipitation (IP) was directed toward the C terminus, which is lacking in the *Lmnb1*$^{\Delta/\Delta}$ cells, and therefore, the IP samples of these cell lysates contained neither lamin B1 nor Oct-1 (Fig. 1 B). This provides evidence of a direct interaction between lamin B1 and Oct-1. This was also confirmed by expressing fluorescently tagged Oct-1 in WT and *Lmnb1*$^{\Delta/\Delta}$ cells. Oct-1 is observed at the nuclear periphery in WT cells but not in the *Lmnb1*$^{\Delta/\Delta}$ cells (Fig. 1 C and Fig. S1, available at http://www.jcb.org/cgi/content/full/jcb.200804155/DC1). Fluorescence loss in photobleaching (FLIP) reveals that Oct-1–EGFP shows very slow turnover when expressed in WT cells, with only 8% being exchanged within 100 s (Fig. 1 D). The turnover is faster in *Lmnb1*$^{\Delta/\Delta}$ cells, in which 43% of Oct-1–EGFP is being exchanged within the same time frame. This experiment shows that the stability of Oct-1 association is tighter in the presence of full-length lamin B1 than in the absence of the latter's C terminus.

To test whether the FLIP results are caused by a tight association between Oct-1 and lamin B1, we performed fluorescence resonance energy transfer (FRET) confocal microscopy using the acceptor photobleach method. In brief, the method involves photobleaching an acceptor fluorophore (e.g., Cy3) and looking for an increase in the fluorescence signal detected for the donor (e.g., EGFP). An increase in the donor fluorescence expressed as the FRET efficiency (see Materials and methods) indicates that the two proteins are indeed within 1–10 nm of each other and thus likely interact directly. In this case, the donor was Oct-1–EGFP, and the acceptor was lamin B1 or lamin A/C detected with Cy3-conjugated secondary antibodies. The Förster radius (at which FRET efficiency is half-maximal) is 6.0 nm for the GFP-Cy3 FRET pair (Wouters and Bastiaens, 1999). Using this approach, we found that the fluorescence of Oct-1–EGFP increases after the bleaching of Cy3 used for lamin B1 detection (FRET efficiency of 4.6%; $n = 20$; Fig. 1 E). However, in the negative control, photobleaching of Cy3 used for lamin A/C detection does not result in an increase in Oct-1–EGFP fluorescence ($P < 0.001$; Fig. 1 E), confirming the absence of an Oct-1–lamin A FRET signal.

Increased available nucleoplasmic Oct-1 in *Lmnb1*$^{\Delta/\Delta}$ cells

Next, we wanted to investigate whether the Oct-1–lamin B1 association and its loss in *Lmnb1*$^{\Delta/\Delta}$ cells has any functional consequences. Electrophoretic mobility shift assay (EMSA) with a fluorescently labeled Oct-1 consensus oligonucleotide (FAM–Oct-1) was performed using equal amounts of nuclear extracts from WT, *Lmnb1*$^{\Delta/\Delta}$, and *Oct1*$^{-/-}$ cells (Fig. 2). A band shift is observed with the WT and *Lmnb1*$^{\Delta/\Delta}$ but not with the *Oct1*$^{-/-}$ nuclear extracts. Furthermore, the intensity of the band obtained with *Lmnb1*$^{\Delta/\Delta}$ extracts is more than that with the WT extracts, suggesting that Oct-1, which has lost its association with the nuclear lamina in *Lmnb1*$^{\Delta/\Delta}$ cells, is now available for binding to its DNA target sequences.

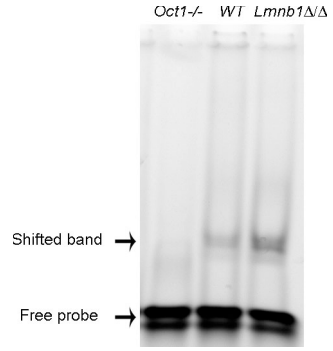

Figure 2. **Oct-1 that is released from the nuclear lamina in *Lmnb1*$^{\Delta/\Delta}$ cells is more readily available to bind to its target DNA sequences.** EMSA was performed using a FAM-labeled Oct-1 consensus-binding oligonucleotide. A band shift is observed in both WT and *Lmnb1*$^{\Delta/\Delta}$ but not in *Oct1*$^{-/-}$ nuclear extracts. The intensity of the shifted band using the *Lmnb1*$^{\Delta/\Delta}$ extract is also increased (relative intensity of shifted band in *Lmnb1*$^{\Delta/\Delta}$ compared with WT = 1.94 in this representative experiment), indicating that the Oct-1 that is released from the nuclear lamina is available to occupy more of its targets.

Gene expression changes in Oct-1– and lamin B1–deficient cells

Although the aforementioned experiments show that Oct-1 released from the nuclear lamina in the absence of full-length lamin B1 is now available to bind to its target sequences, they do not prove that this has any consequence in terms of gene expression of Oct-1 targets. To establish this, we first wanted to identify Oct-1 targets that are dysregulated in the *Lmnb1*$^{\Delta/\Delta}$ cells (i.e., genes that are dependent on both lamin B1 and Oct-1 for their normal expression). We compared the gene expression patterns of *Lmnb1*$^{\Delta/\Delta}$ with WT cells using six biological replicates of each and six hybridizations performed with dye swaps. We had previously identified 790 dysregulated genes ($P < 0.05$ using CyberT) in the absence of normal full-length lamin B1 (ArrayExpress accession no. E-MEXP-538). CyberT is a web-based implementation of a Bayesian probabilistic framework for the analysis of microarray data designed for the analysis of data with high measurement noise and variability and typically low replicate numbers (Baldi and Long, 2001). This Bayesian approach has been shown to be more appropriate for the analysis of microarray data than the significance analysis of microarray (Tusher et. al., 2001) program and the Student's t test when n is small (Choe et al., 2005), although this difference is reduced when $n > 5$ as in our experiments (Baldi and Long, 2001).

We compared the gene expression changes in the *Lmnb1*$^{\Delta/\Delta}$ cells with those previously reported in *Oct1*$^{-/-}$ cells

Downloaded from http://rupress.org/jcb/article-pdf/184/1/45/1555786/jcb_200804155.pdf by guest on 08 February 2026

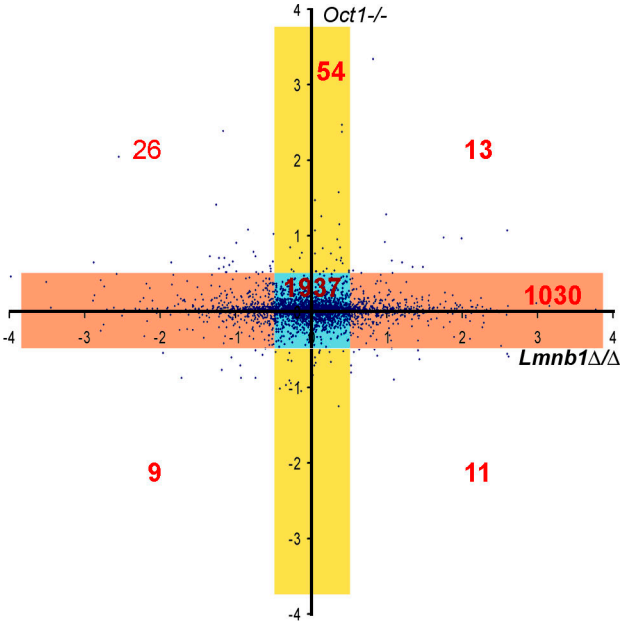

Figure 3. **A scatter plot of the $\log_2$ fold changes of genes in *Oct1*$^{-/-}$ and *Lmnb1*$^{\Delta/\Delta}$ cells.** The shaded areas show genes that are either unchanged or moderately dysregulated as defined by a 0.5 cutoff. Only 54 genes are significantly dysregulated in Oct-1–deficient cells and not in *Lmnb1*$^{\Delta/\Delta}$ cells (yellow), whereas 1,030 genes are dysregulated in *Lmnb1*$^{\Delta/\Delta}$ cells and not in Oct-1–deficient cells (orange). Genes outside the shaded areas are those that are significantly dysregulated in both deficient cell types (i.e., the regulation of which is dependent on both Oct-1 and lamin B1). There are also 1,937 genes that are not dysregulated in either cell type (central blue region).

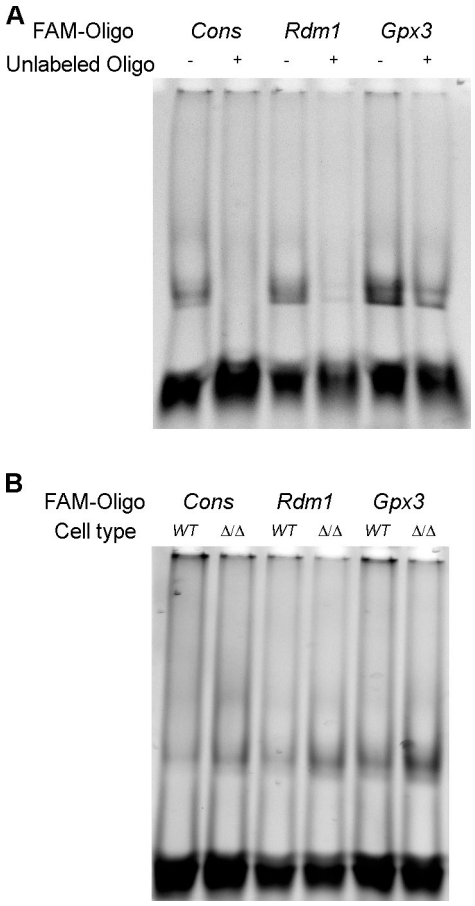

Figure 4. **Oct-1 can bind to its target sequences within the regulatory regions of genes that are dysregulated in both Oct-1– and lamin B1–deficient cells.** (A) Oct-1 in nuclear extracts from *Lmnb1*$^{\Delta/\Delta}$ cells show band shifts using a consensus Oct-1–binding oligonucleotide (Cons) as well as predicted Oct-1–binding sequences in the promoter regions of *Rdm1* and *Gpx3*. The specificity of binding is confirmed by including an excess of nonlabeled consensus oligonucleotide (+ lanes), which reduces the intensity of the shifted bands. (B) The shifted bands are more intense in the case of *Lmnb1*$^{\Delta/\Delta}$ extracts as a result of the release of Oct-1 from the nuclear lamina. Relative intensity values (*Lmnb1*$^{\Delta/\Delta}$/WT) are 2.44 for *Rdm1* and 1.68 for *Gpx3*. Similar results were obtained using the Oct-1–binding sequences of *Mgst1* and *Mmp13* (Fig. S3, available at http://www.jcb.org/cgi/content/full/jcb.200804155/DC1).

(Gene Expression Omnibus [GEO] accession no. GDS1446; Tantin et al., 2005). We found that 1,937 genes are unchanged in both cell types and are therefore independent of Oct-1 or lamin B1 (Fig. 3, blue region). 54 genes were dysregulated in *Oct1*$^{-/-}$ but not in *Lmnb1*$^{\Delta/\Delta}$ cells and are thus dependent on Oct-1 but not lamin B1 for their expression (Fig. 3, yellow regions), whereas 1,030 genes were dysregulated in *Lmnb1*$^{\Delta/\Delta}$ and not *Oct1*$^{-/-}$ cells, implying that their expression is dependent on lamin B1 but not Oct-1 (Fig. 3, orange regions). The 57 genes in the white quadrants (Fig. 3) represent those that are dysregulated in both cell types and are therefore dependent on both Oct-1 and lamin B1 for their expression (Table S2, available at http://www.jcb.org/cgi/content/full/jcb.200804155/DC1). To assess the significance of finding this number of genes altered in both experimental conditions, the bootstrapping method was used with 500,000 samples (see Materials and methods). This method shows that the probability of a chance observation of 57 genes that are changed in both experiments is <0.00012 (Fig. S3).

EMSA and chromatin IP (ChIP)

We selected some of the genes identified as Oct-1 targets using the aforementioned gene expression analysis to test whether they have functional Oct-1–binding sites. Putative Oct-1–binding sites within the promoter regions of the genes were selected using an online version of a hidden Markov profile comparison tool (multigenome analysis of positions and patterns of elements of regulation [MAPPER]; http://bio.chip.org/mapper; Fig. S4, available at http://www.jcb.org/cgi/content/full/jcb.200804155/DC1; Marinescu et al., 2005). EMSA using FAM-labeled oligonucleotide duplexes with the predicted Oct-1–binding sequences of *Rdm1*, *Gpx3*, *Mgst1*, and *Mmp13* confirms that the sequences can specifically bind Oct-1 because the intensities of the shifted bands are reduced by the inclusion of a nonlabeled oligonucleotide with the Oct-1 consensus sequence in the assay (Fig. 4 A). Increased intensities of the shifted bands are also observed in the *Lmnb1*$^{\Delta/\Delta}$ cell extract assays compared with the WT cell extracts, further confirming that there is an elevated amount of free Oct-1 in the *Lmnb1*$^{\Delta/\Delta}$ cells that can bind to its target sequences in the promoter regions of the tested genes (Fig. 4 B and Fig. S2).

To confirm that this is occurring in the *Lmnb1*$^{\Delta/\Delta}$ cells, we performed ChIP using anti–Oct-1 on WT and *Lmnb1*$^{\Delta/\Delta}$ cells and determined the relative enrichment of Oct-1 occupancy of potential targets using quantitative real-time PCR

Downloaded from http://rupress.org/jcb/article-pdf/184/1/45/1555786/jcb_200804155.pdf by guest on 08 February 2026

A

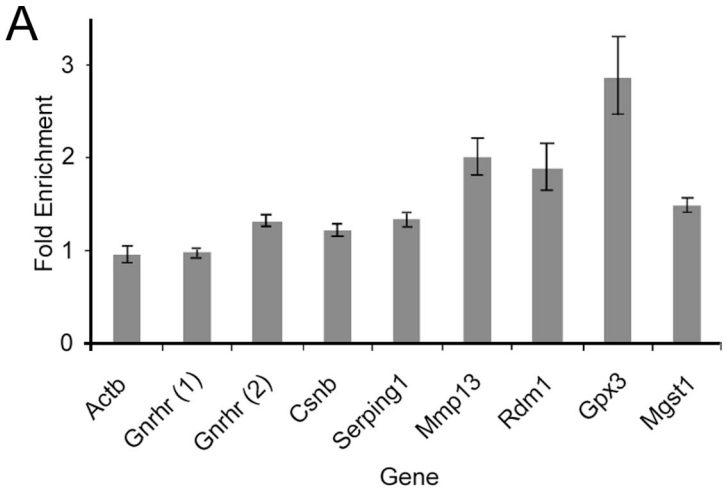

B

Gene	Expression fold change		ChIP fold enrichment	MAPPER score	MAPPER E-value	MAPPER model
	Oct-1-/-	*Lmnb*Δ/Δ				
Mgst1	2	-1.13	1.48	5.4	7.7	M00453
Gnrhr (1)	0.06	-1.70	0.97	2.4	47	M00930
Gnrhr (2)	0.06	-1.70	1.31	2 (a)	20	M00135
				11.2 (b)	0.18	M00135
Serping1	4.7	-1.5	1.32	1.8	24	M00162
Rdm1	3.6	-1.05	1.88	4.6	13	M00135
Gpx3	2.6	-1.65	2.85	5.3	9.8	M00135
Mmp13	0.02	1.6	2.00	3.5	15	M00137
Csnb	0.01	0.68	1.22	4.7	1.3	M00162

C

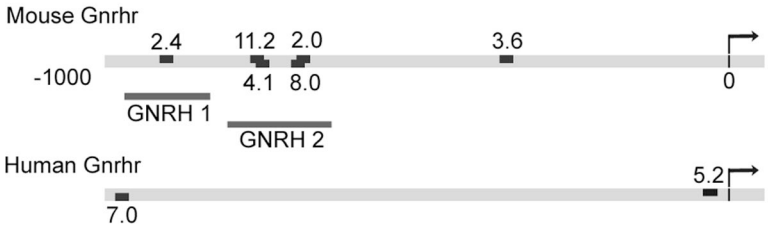

Figure 5. **Enrichment of Oct-1 binding to target sequences in *Lmnb1*$^{\Delta/\Delta}$ cells.** After ChIP of *Lmnb1*$^{\Delta/\Delta}$ and WT cells using an anti–Oct-1 antibody, target genes were detected by quantitative real-time PCR as described in Materials and methods. All targets showed significant enrichment of Oct-1 binding ($P < 0.05$) except for *Gnrhr* 1. (A and B) Note that the *Actb* sequence does not have an Oct-1–binding sequence, and thus, no enrichment in binding is detected. The MAPPER scores and E values as well as the MAPPER Oct-1–binding models are also shown for the Oct-1–binding sites that were analyzed using ChIP. (C) The mouse *Gnrhr* promoter region has several potential Oct-1–binding sites. Two sets of primers producing two PCR products were used to examine the occupancy of Oct-1 in the *Gnrhr* promoter. *Gnrhr* 2 was enriched, whereas *Gnrhr* 1 was not, suggesting that Oct-1 preferentially binds to the sequences within *Gnrhr* 2. Data shown are from two separate nuclear extracts assayed in triplicate and are means ± SD. Sequence alignment data are provided in Fig. S4 (available at http://www.jcb.org/cgi/content/full/jcb.200804155/DC1).

(qRT-PCR). We selected seven genes for ChIP analysis, including genes previously shown to be regulated by Oct-1 gonadotropin-releasing hormone receptor (*Gnrhr*) and genes identified in this study as both Oct-1 and lamin B1 dependent. Increases in Oct-1 occupancy of the predicted binding sites of *Csnb*, *Mmp13*, *Rdm1*, *Gpx3*, *Mgst1*, and *Serping1* were detected in the *Lmnb1*$^{\Delta/\Delta}$ cells relative to the WT cells, whereas no relative increase in occupancy was detected for β-actin, which does not have an Oct-1–binding site (Fig. 5 A). Interestingly, the Oct-1 site in the *Gnrhr* promoter previously identified using a mobility shift assay showed no change in Oct-1 occupancy *Gnrhr* 1. To understand this unexpected discrepancy, we examined the *Gnrhr* promoter region using MAPPER and found additional predicted Oct-1–binding sites with much higher scores (Fig. 5 B). When we repeated the ChIP/qRT-PCR experiment using primer pairs selective for the highest scoring Oct-1 site, we found a significant change in occupancy (Fig. 5, compare *Gnrhr* 1 with *Gnrhr* 2).

Lmnb1$^{\Delta/\Delta}$ cells are more susceptible to oxidative stress

Some of the genes that are dysregulated in Oct-1 and *Lmnb1*$^{\Delta/\Delta}$ cells are involved in cellular responses to oxidative stress, as shown in Table I. The Oct-1–deficient cells have already been shown to harbor elevated ROS levels and be more susceptible to oxidative stress (Tantin et al., 2005). Cell survival assays in the presence of H_2O_2 showed that the *Lmnb1*$^{\Delta/\Delta}$ cells are also more susceptible to oxidative stress (Fig. 6 A). Using the

Downloaded from http://rupress.org/jcb/article-pdf/184/1/45/1555786/jcb_200804155.pdf by guest on 08 February 2026

Table I. **Fold changes of genes involved in oxidative stress responses**

Gene	Fold change		References
	In *Oct1*$^{-/-}$ [a]	In *Lmnb1*$^{\Delta/\Delta}$ [b]	
Peroxiredoxin 2 (*Prdx2*)	10.2	0.8	Sanchez-Font et al., 2003[c]
Serine (or cysteine) proteinase inhibitor, clade G, member 1 (*Serping1*)	4.7	−1.5	Tantin et al., 2005
RAD52 motif 1 (*Rdm1*)	3.6	−1.05	Tantin et al., 2005
Glutathione peroxidase 1 (*GPx1*)	0.2	0.4	Fu et al., 2001[c]
Glutathione peroxidase 3 (*Gpx3*)	2.6	−1.65	Ouyang et al., 2005
Tissue inhibitor of metalloproteinase 3 (*Timp3*)	2.53	−0.72	Winokur et al., 2003[c]
Interleukin 6 (*Il-6*)	2.48	−3.8	Orosz et al., 2007
Growth arrest specific 6 (*Gas6*)	2.04	−0.50	Valverde, 2005
Growth arrest specific 5 (*Gas5*)	−3.52	0.01	Tantin et al., 2005
Superoxide dismutase 1, soluble (*Sod1*)	2	−0.4	Ali et al., 2006[c]
Selenoprotein P, plasma, 1 (*Sepp1*)	2	−1.13	Steinbrenner et al., 2006[c]
GST, mu 1 (*Gstm1*)	2	−0.6	Aydemir et al., 2007[c]
GST, mu 2 (*Gstm2*)	2	−2	Tantin et al., 2005
Microsomal GST (*Mgst*)	0.5	−4	Hayes and Strange, 2000
Glutamate cysteine ligase (γ-glutamyl-cysteine synthetase), regulatory (*Glclr*)	0.3	−0.4	Rozet et al., 1998

Log fold changes with $P < 0.05$ are shown.

[a]Data from Tantin et al., 2005.

[b]Log_2 fold ratios.

[c]Reports of down-regulation being associated with increased susceptibility to ROS.

cell-permeable probe 2′,7′-dichlorodihydrofluorescein diacetate (H_2DCFDA) for ROS level detection (Sanchez Ferrer et al., 1990), the *Oct1*$^{-/-}$ and *Lmnb1*$^{\Delta/\Delta}$ cells were found to have significantly elevated levels of ROS compared with the WT cells (Fig. 6, B and C). To demonstrate that this change was directly dependent on lamin B1 function, we reduced its expression acutely in WT cells using *Lmnb1* siRNA (Fig. 6, B and C). Cells in which lamin B1 levels were reduced showed increased ROS levels (Fig. 6 C). This effect is not a consequence of siRNA transfection per se because a control siRNA had no effect on ROS levels (Fig. 6 D). As a further control, we repeated ROS measurements in *Lmnb1*$^{\Delta/\Delta}$ cells after restoration of lamin B1 expression (by transfecting cells to express full-length lamin B1) and showed that ROS levels were decreased to WT levels in those transgenic fibroblasts that were expressing lamin B1 (Fig. 6 E).

ROS levels were also reduced to near WT levels in *Lmnb1*$^{\Delta/\Delta}$ cells, whereas Oct-1 levels were reduced using *Oct1* siRNA (Fig. 6 C). Furthermore, reduction of Oct-1 levels in *Lmnb1*$^{\Delta/\Delta}$ cells reduced their susceptibility to oxidative stress, whereas overexpression of Oct-1 in WT cells increased their susceptibility in comparison with cells that are transfected with a control siRNA or a control EGFP construct (H2B-EGFP), respectively (Fig. 7 A). These experiments indicate that the elevated ROS levels and susceptibility to oxidative stress in the *Lmnb1*$^{\Delta/\Delta}$ cells is indeed mediated by Oct-1.

Further support for a direct effect of Oct-1 comes from experiments in which Oct-1 levels in *Lmnb1*$^{\Delta/\Delta}$ cells are reduced by siRNA. Fig. 7 B (white bars) shows the effect of *Oct1* siRNA on the expression of three genes that are involved in the response to oxidative stress. Two of the genes (*Gpx3* and *Rdm1*) are normally repressed by Oct-1 (and therefore are down-regulated in the *Lmnb1*$^{\Delta/\Delta}$ cells); this down-regulation is reversed when Oct-1 is lowered by siRNA (i.e., control siRNA–normalized fold change greater than one). Similarly, a gene that is activated by Oct-1 and thus up-regulated in *Lmnb1*$^{\Delta/\Delta}$ cells (*Mmp13*) shows a reversal of this effect when Oct-1 is reduced by siRNA (i.e., control siRNA–normalized fold change less than one). Final confirmation that this is a direct effect of Oct-1 comes from the converse experiment in which Oct-1 is independently overexpressed in WT cells (Fig. 7 B, gray bars). In this case, the genes normally repressed by Oct-1 (*Gpx3* and *Rdm1*) are down-regulated by Oct-1 overexpression, whereas the gene normally activated by Oct-1 shows increased expression.

Discussion

Given that not all of the gene expression changes observed in the absence of full-length lamin B1 could be explained by altered chromatin–lamina interactions (Malhas et al., 2007), we sought additional mechanisms. In particular, it has previously been reported that Oct-1 colocalizes with lamin B and that the dissociation of Oct-1 from the nuclear periphery results in the up-regulation of the collagenase gene (Imai et al., 1997). Therefore, we considered the possibility that some of the gene expression changes observed in the *Lmnb1*$^{\Delta/\Delta}$ cells might be a result of the dissociation of Oct-1 from the nuclear lamina in the absence of full-length lamin B1.

We first showed that Oct-1 associates with lamin B1, that the loss of this interaction leads to elevated Oct-1 levels in the nucleoplasm, and that the released Oct-1 can bind to its consensus target sequences. We then wanted to investigate whether this increased binding can have a functional effect and therefore sought to identify the genes that are dysregulated in the *Lmnb1*$^{\Delta/\Delta}$

Downloaded from http://rupress.org/jcb/article-pdf/184/1/45/1555786/jcb_200804155.pdf by guest on 08 February 2026

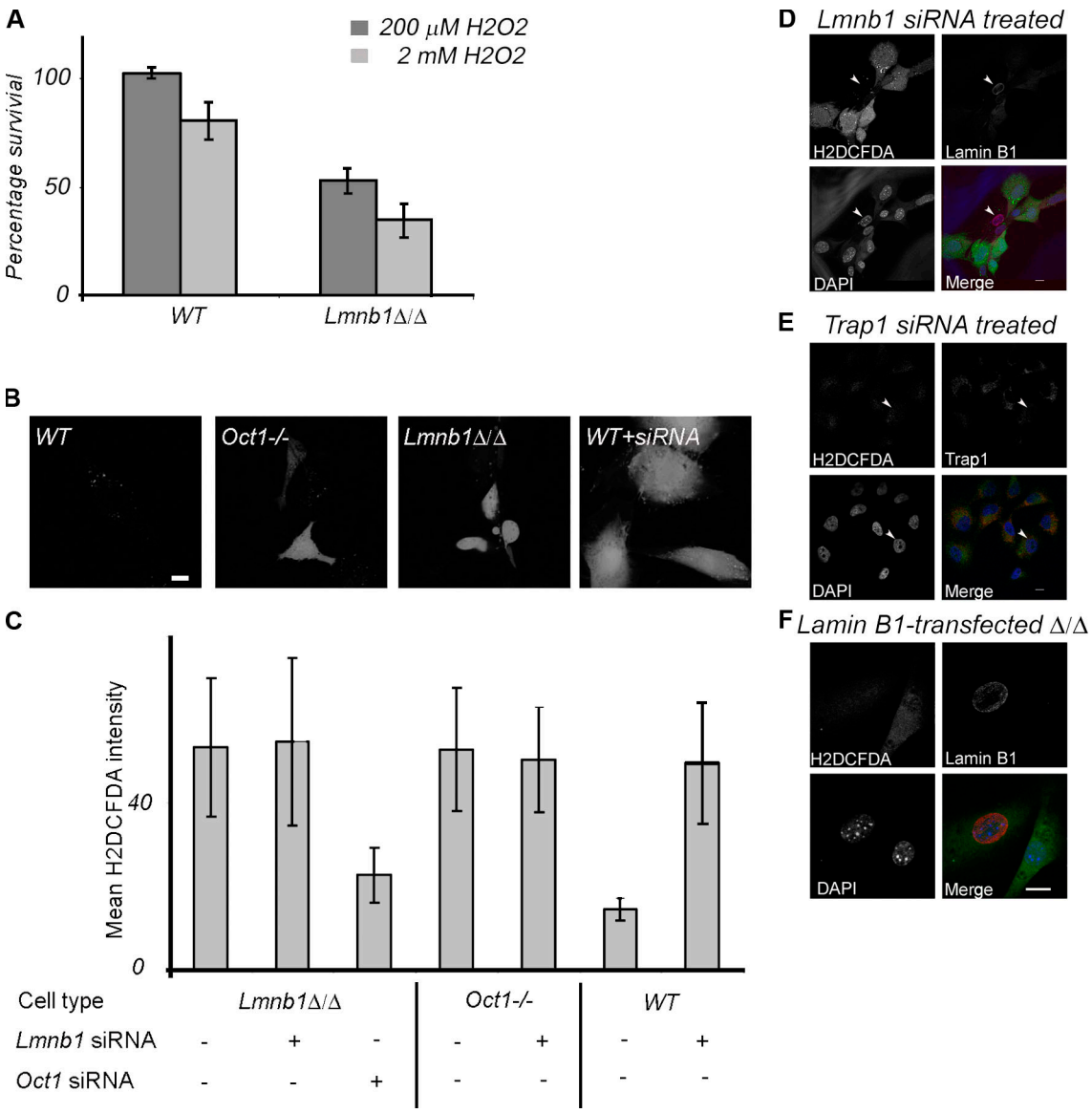

Figure 6. ***Lmnb1*$^{\Delta/\Delta}$ cells are more susceptible to oxidative stress and harbor high levels of ROS.** (A) Percentages represent viable cell counts for treated wells relative to untreated wells of cells of the same type assayed in parallel. *Lmnb1*$^{\Delta/\Delta}$ cells are significantly more susceptible to oxidative stress than WTs ($P < 0.001$ by Student's *t* test). (B) The cell-permeable fluorogenic probe H_2DCFDA was used for intracellular ROS detection. *Oct1*$^{-/-}$, *Lmnb1*$^{\Delta/\Delta}$, and *Lmnb1* siRNA–treated WT cells show a significantly more intense fluorescent signal after treatment with the dye, indicating that they have higher levels of ROS than the untreated WT cells. (C) Quantitation of ROS levels in WT, *Oct1*$^{-/-}$, and *Lmnb1*$^{\Delta/\Delta}$ cells before and after treatment with *Lmnb1* siRNA, showing that ROS levels are elevated in the mutant cells and after a reduction of lamin B1 expression in the WT cells. ROS levels are also normalized to near WT levels in *Oct1* siRNA–treated *Lmnb1*$^{\Delta/\Delta}$ cells. 50 cells were analyzed for each condition. (D) WT cells were transfected with *Lmnb1* siRNA. ROS levels (green) and lamin B1 (red) were measured 48 h after transfection. Cells showing reduced levels of lamin B1 expression have higher levels of ROS. The arrowheads show a lamin B1–expressing cell that has lower ROS levels compared with the surrounding cells. (E) Cells transfected with a control siRNA (Trap1) do not show elevated levels of ROS. The arrowheads indicate examples of a cell with reduced Trap1 expression and no increase in ROS levels. (F) Transfecting *Lmnb1*$^{\Delta/\Delta}$ cells to express full-length lamin B1 (red) reduces the levels of ROS, indicating that the effect on ROS levels in the *Lmnb1*$^{\Delta/\Delta}$ cells is directly linked to the loss of full-length lamin B1 expression. Mean ± SD values are shown ($P < 0.001$ by analysis of variance). Bars, 10 μm.

cells as a result of the altered Oct-1 distribution. To test this, we made use of existing data on gene expression in murine Oct-1 knockout cells (Tantin et al., 2005). We found that 1,030 genes are either unchanged or moderately dysregulated in the absence of Oct-1 but are significantly dysregulated in the absence of full-length lamin B1, indicating a dependence on lamin B1 but not Oct-1. This group includes most of the small number of genes we identified as dependent on processed lamin B1 (Malhas et al., 2007) but must also include many genes whose lamin B1 dependence cannot be accounted for by either lamin B1–chromatin interactions or lamin B1–Oct-1 interactions. Efforts are continuing to identify the mechanism by which lack of a stable B-type lamina affects expression of these genes. Only 54 genes are dependent on Oct-1 and not lamin B1 for their normal expression. We surmise that these represent genes with a stringent requirement for low levels of Oct-1 and that in both WT and *Lmnb1*$^{\Delta/\Delta}$ cells, the Oct-1 level exceeds this permissive requirement. We identified 57 genes that are dependent on both lamin B1 and Oct-1 for their normal expression. Several of these genes have been found to be involved in the response to

Downloaded from http://rupress.org/jcb/article-pdf/184/1/45/1555786/jcb_200804155.pdf by guest on 08 February 2026

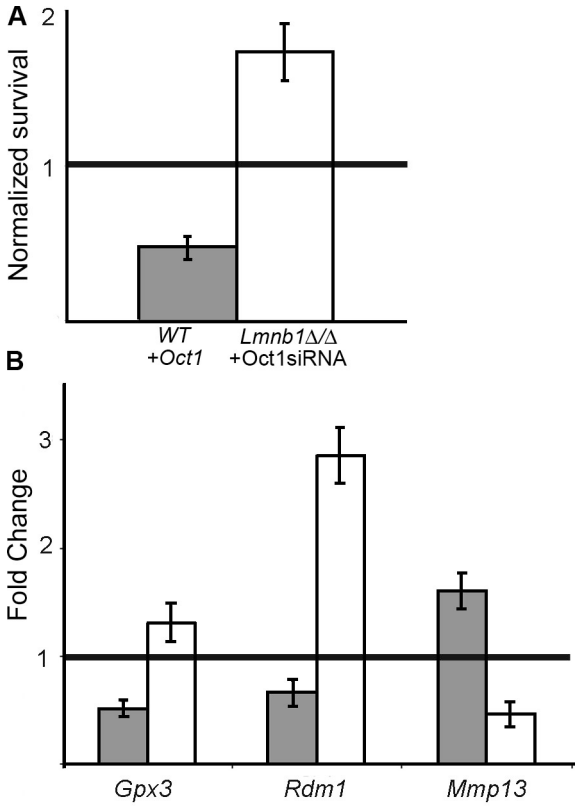

Figure 7. **The dysregulated gene expression and susceptibility to oxidative stress in the lamin B1–deficient cells are mediated by Oct-1.** (A) WT cells were transfected with Oct-1–EGFP or H2B-EGFP as a control (gray bar), whereas *Lmnb1*$^{\Delta/\Delta}$ cells were transfected with *Oct1* siRNA or a control siRNA (white bar). After treatment with 2 mM H_2O_2, cell survival assays were performed as described in Materials and methods. The normalized cell survival is a ratio of percent cell survival of the treated versus control cells. A ratio >1, as in the case of the *Lmnb1*$^{\Delta/\Delta}$ cells where Oct-1 levels have been reduced, reflects an improvement of cell survival. A ratio <1, as in the case of the WT cells overexpressing Oct-1, reflects a reduction in cell survival. Overexpression of Oct-1 in the WTs increases their susceptibility, whereas reduction of Oct-1 levels in the *Lmnb1*$^{\Delta/\Delta}$ cells reduces their susceptibility, demonstrating that the sensitivity to oxidative stress in the lamin B1–deficient cells is mediated by Oct-1. (B) The expression levels of *Gpx3*, *Rdm1*, and *Mmp13* in WT cells transfected with Oct-1–EGFP (gray bars) and *Lmnb1*$^{\Delta/\Delta}$ cells transfected with *Oct1* siRNA (white bars) were measured and are presented as fold changes versus the relevant controls. The results show that overexpression of Oct-1 in the WTs or the reduction of its levels in the lamin B1–deficient cells reverses the gene expression patterns of these genes, which are involved in the response to oxidative stress. The horizontal lines indicate a ratio of 1, which is where the bars would be if no changes in gene expression or susceptibility in comparison with the controls were observed. Data are means ± SD of three independently performed replicates.

oxidative stress (Tantin et al., 2005). 15 of these genes are also dysregulated in the *Lmnb1*$^{\Delta/\Delta}$ cells (Table I). If the hypothesis that Oct-1 is released from sequestration in *Lmnb1*$^{\Delta/\Delta}$ cells is correct, we would expect Oct-1–dependent genes to show expression changes in opposite directions in *Oct1*$^{-/-}$ and *Lmnb1*$^{\Delta/\Delta}$ cells. This is true for 13 of the 15 genes involved in oxidative stress responses. At first glance, one might expect the resulting phenotypes to be opposite (i.e., if there is increased vulnerability to oxidative stress in *Oct1*$^{-/-}$ cells, there would be reduced vulnerability in *Lmnb1*$^{\Delta/\Delta}$ cells). However, it is important to note that for six of these genes there is already published evidence that either increased or decreased expression increases vulnerability to oxidative stress (Table I). It is worth noting that the increased Oct-1 occupancy, target gene dysregulation, and the resulting phenotype are caused by Oct-1 release and not its overexpression because the expression of the *Oct1* gene itself is unchanged in the *Lmnb1*$^{\Delta/\Delta}$ cells compared with the WTs (both at transcript level and protein level; Fig. 1 A).

Oct-1 is known to have repressive as well as activating effects on gene expression. Oxidative stress response genes that are dysregulated in the *Oct1*$^{-/-}$ cells are mostly down-regulated in the *Lmnb1* $^{\Delta/\Delta}$ cells (Table I), suggesting that in the WT cells, Oct-1 is sequestered by lamin B1, and thus the oxidative stress response genes that have octamer sequences are expressed at normal levels. In the *Lmnb1* $^{\Delta/\Delta}$ cells, where there are higher levels of nucleoplasmic Oct-1 as a result of the loss of the sequestration by lamin B1, Oct-1 moves away from the periphery, binds to the octamer sequences, and down-regulates the target genes involved in response to oxidative stress, which we detect using EMSA, ChIP, and microarray, respectively. As a result, the *Lmnb1* $^{\Delta/\Delta}$ cells harbor high levels of ROS and are more susceptible to oxidative stress. Other examples of genes that are repressed by Oct-1 are the *Gnrhr* gene (Cheng et al., 2002) and the vascular cell adhesion molecule 1 (Vcam1; dela Paz et al., 2007), which are also down-regulated in the *Lmnb1* $^{\Delta/\Delta}$ cells (fold ratios of 0.3 and 0.7, respectively).

The *Gnrhr* gene offers a further interesting insight. An Oct-1–binding site has previously been identified and confirmed using an in vitro mobility shift assay (Cheng et al., 2002), but our ChIP/qRT-PCR analysis failed to detect a change in occupancy at this site in *Lmnb1* $^{\Delta/\Delta}$ cells, whereas all other sites tested showed an increase in Oct-1 occupancy. However, this site is very weakly predicted as an Oct-1–binding site by the MAPPER algorithm, and much stronger Oct-1 sites are predicted elsewhere in the promoter region of *Gnrhr* (Fig. 5 C). When we repeated ChIP and qRT-PCR using primers designed to detect these additional predicted Oct-1 sites, we found a significant increase in Oct-1 occupancy in *Lmnb1* $^{\Delta/\Delta}$ cells. We conclude that the relatively modest increase in nucleoplasmic Oct-1 protein levels between WT and *Lmnb1*$^{\Delta/\Delta}$ cells has enabled us to detect subtle differences in the behavior of different Oct-1–binding sites in the same promoter. Fig. 5 B shows site occupancy changes ranging from 1.22 in *Csnb* to 2.85 in *Gpx3*, indicating that different Oct-1 sites respond differently to the same increase in Oct-1 level. Because the elevated binding is observed in the EMSA on short duplexes, they cannot depend on the sequence context and steric effects of transcription factor binding to adjacent sites. Moreover, because these differences are still detected by ChIP, they are not abrogated by transcription factor binding in a wider sequence context in intact nuclei.

Oct-1 is also known to function as an activator of expression of some targets, such as the U6 small nuclear RNA and osteopontin (*Opn* or *Spp1*; Botquin et al., 1998; Remenyi et al., 2002), which are both up-regulated in the *Lmnb1*$^{\Delta/\Delta}$ cells (fold ratios of 1.7 and 10, respectively). Again, this can be explained by the loss of Oct-1 sequestration and an increase in nucleoplasmic Oct-1, which is now available to promote the transcription of such genes. Imai et al. (1997) observed that an up-regulation

Downloaded from http://rupress.org/jcb/article-pdf/184/1/45/1555786/jcb_200804155.pdf by guest on 08 February 2026

of the human interstitial collagenase gene accompanied the loss of Oct-1 from the nuclear periphery during cellular aging. We also observe an up-regulation in the mouse interstitial collagenase gene *Mmp13* and an elevated level of Oct-1 occupancy of the Oct-1–binding sequence in its promoter region.

Elevated levels of ROS result in modifications to proteins, lipids, and DNA that are associated with aging (for review see Finkel and Holbrook, 2000), a process that is also linked to defects in nuclear envelope components. Alterations to the nuclear architecture are observed during the normal aging process (Wilson, 2005; Scaffidi and Misteli, 2006), and an extended lifespan in *Caenorhabditis elegans* has been associated with increased nuclear envelope integrity (Haithcock et al., 2005). Furthermore, mutations in genes coding for nuclear structural components such as lamin A are associated with several diseases, including the premature aging disorder Hutchinson-Gilford progeria syndrome (Eriksson et al., 2003). Several of the abnormalities resulting from nuclear structure defects in both an animal model and cells in culture can be reversed by treatment with farnesyltransferase inhibitors that act by normalizing the nuclear architecture (Glynn and Glover, 2005; Toth et al., 2005; Yang et al., 2006). Thus, there is mounting evidence that nuclear architecture and aging are interrelated and that compromised nuclear architecture might play a central role in the aging process (Haithcock et al., 2005; Wilson, 2005), although the exact mechanisms have yet to be unraveled. The findings we present in this study advance our understanding of this mechanism by demonstrating that disrupting the interactions between lamin B1 and Oct-1 result in the overall down-regulation of oxidative stress response genes and elevated ROS levels, both of which are hallmarks of the normal aging process.

Materials and methods

Cell culture, constructs, and sequential nuclear extraction

Lamin B1 WT and *Lmnb1*$^{\Delta/\Delta}$ cells were obtained from S. Young (University of California Los Angeles, Los Angeles, CA) and M. Bergö (Sahlgrenska Center for Cardiovascular and Metabolic Research, Göteborg, Sweden), whereas *Oct1*$^{-/-}$ cells were provided by D. Tantin (University of Utah, Salt Lake City, UT). All mouse embryonic fibroblasts were cultured in DME supplemented with 10% FCS, L-glutamine, and nonessential amino acids. For cell survival assays, cells were seeded 24 h before treatment with 200 µM or 2 mM H_2O_2 for 24 h. Viable cells were quantified using the CellTiter-Blue cell viability assay (Promega) or manually using a Neubauer hemocytometer (Thermo Fisher Scientific). DNA transfections were performed using Lipofectamine 2000 (Invitrogen), whereas siRNA transfections were performed using transfection reagent (HiPerFect; QIAGEN). All experiments were performed 48 h after transfection. *Oct1*, *Lmnb1*, and control siRNA were purchased from Applied Biosystems. Full-length GFP-tagged lamin B1 used in this study has been described previously (Maske et al., 2003). The Oct-1–EGFP construct was provided by S. Murphy (University of Oxford, Oxford, England, UK). Differential nuclear extraction was adapted from the method described previously by Otto et al. (2001). In brief, purified nuclei were resuspended in nuclear isolation buffer (10 mM Hepes, pH 7.4, 2 mM $MgCl_2$, 25 mM KCl, 250 mM sucrose, 1 mM DTT, and a protease inhibitor cocktail; Sigma-Aldrich) and sonicated for two 5-s bursts at a 10-µm amplitude. Insoluble material was pelleted at 20,000 *g* for 5 min, resuspended in nuclear extraction buffer (20 mM Hepes, pH 7.4, 1 M NaCl, and protease inhibitor cocktail), and incubated at room temperature with agitation for 20 min. The extraction was repeated using nuclear extraction buffer with 2% Triton X-100 and 4 and 8 M urea in sequential extractions.

IP

Cells were lysed using radio IP assay lysis buffer in the presence of complete protease inhibitor cocktail (Roche). Lysates were precleared twice using protein G PLUS-Agarose (Santa Cruz Biotechnology, Inc.) and immunoprecipitated overnight at 4°C using goat anti–lamin B1 (Santa Cruz Biotechnology, Inc.). IP complexes were captured using protein G PLUS-Agarose, eluted using Laemmli loading buffer, and analyzed by Western blotting using anti–lamin B1 (Santa Cruz Biotechnology, Inc.), anti–Oct-1 (Santa Cruz Biotechnology, Inc.), or donkey anti–goat HRP conjugate (Jackson ImmunoResearch Laboratories).

RNA isolation and gene expression analysis

RNA isolation, gene expression analyses, and validation have been described previously (Malhas et al., 2007). Full details of the slide layout, culture conditions, detailed protocols, and primary extracted data files have been submitted to ArrayExpress (ArrayExpress accession no. E-MEXP-538). The Oct-1 dataset was downloaded from the GEO database, uploaded to BioArray Software Environment (Saal et al., 2002), and analyzed with the lamin B1 dataset for all comparisons.

To calculate the probability of having a particular number of genes changed in both experiments, a repeat sampling bootstrapping method was used. Specifically, for each cycle, 113 genes are randomly drawn from the list of 3,080 common genes, generating set A, and 1,089 genes are drawn randomly from the same 3,080 list, generating set B. Then, the number of genes present in both A and B (*n*) is recorded. After 500,000 cycles, the values of *n* were plotted to give a probability distribution histogram. The probability distribution is shown in Fig. S3.

Immunofluorescent labeling and laser-scanning microscopy

Cells were fixed in 4% PFA and 250 mM Hepes, pH 7.4, on ice for 10 min and in 8% PFA and 250 mM Hepes, pH 7.4, for 50 min at room temperature. Cells were incubated in 25 mM glycine in PBS for 10 min, permeabilized with 0.4% Triton X-100 in PBS for 5 min, and blocked with 0.4% fish skin gelatin in PBS for 30 min at room temperature. Incubations with primary and secondary antibodies were for 1 h each at room temperature. Cells stained with concanavalin A–Alexa Fluor 633 (Con A 633; Invitrogen) were incubated with 100 µg/ml Con A conjugate for 1 h at room temperature. Primary antibodies used were goat anti–lamin B1, mouse monoclonal anti–lamin B1 (8D1; Maske et al., 2003), rabbit anti–Oct-1 (Thermo Fisher Scientific), and mouse anti–lamin A/C (Novocastra). Secondary antibodies used were donkey anti–goat, anti–mouse, and anti–rabbit (Jackson ImmunoResearch Laboratories) conjugated to Alexa Fluor 488, HRP, Cy3, or Cy5. For ROS detection, cells were washed with PBS, incubated with 20 µM H_2DCFDA (EMD) in phenol red-free DME for 30 min, and washed with PBS. All imaging was performed using a microscope (LSM 510 META; Carl Zeiss, Inc.) on an Axio Imager. Z1 (Carl Zeiss, Inc.) with a 63× NA 1.4 oil immersion objective lens. Laser lines used were 405 nm, 488 nm, 543 nm, and 633 nm to excite DAPI, Alexa Fluor 488, Cy3 and Cy5, or Alexa Fluor 633, respectively. Fluorescence was detected using the following filters: base pairs 420–480, base pairs 505–530, base pairs 560–615, and long pass 650. Images were analyzed using MetaMorph (MDS Analytical Technologies) or Image Browser (Carl Zeiss, Inc.) software.

Photobleaching experiments

FLIP was performed as described previously (Malhas et al., 2007) except that an inverted microscope (LSM 510 META) was used. In brief, a region of interest (ROI) was photobleached at full laser power while scanning at 4% laser power elsewhere. For quantitative analysis, background intensity was subtracted, and intensities of a specific ROI outside the photobleached area were measured over time and normalized using intensities of an ROI in a transfected but nonbleached cell.

FRET

FRET using the acceptor photobleaching method (Kenworthy, 2001) was used after immunolabeling of peripheral lamin B1 with 8D1, anti–mouse conjugated to Cy3 was used as the acceptor, and Oct-1–EGFP was used as the donor. An ROI was selected, and both the donor and acceptor were scanned 10 times (1.61 µs/pixel). The ROI was bleached with the 543-nm laser at 100% laser power. This was followed by scanning to detect any changes in the acceptor and donor intensities. FRET efficiency was calculated using the following formula: $100 \times (1-[I_b/I_a])$, where I_b and I_a are the intensities of the donor before and after bleaching, respectively.

ChIP

Cells (~10^6 each of *Lmnb1*$^{+/+}$ and *Lmnb1*$^{\Delta/\Delta}$ cells) were fixed with 1% formaldehyde for 10 min and incubated with 125 mM glycine for 5 min at room temperature. All subsequent washes and lysis steps were performed in the presence of complete protease inhibitor cocktail (Roche). Cells were washed with ice-cold PBS, scraped, pelleted, and lysed with 10 mM Tris,

Downloaded from http://rupress.org/jcb/article-pdf/184/1/45/1555786/jcb_200804155.pdf by guest on 08 February 2026

10 mM NaCl, and 0.2% NP-40, pH 8, on ice for 10 min. Nuclei were pelleted and lysed with nuclear lysis buffer (50 mM Tris, 10 mM EDTA, and 1% SDS, pH 8) on ice for 10 min. Chromatin was sonicated to generate DNA fragments ranging from 300 to 1,000 bp as confirmed by electrophoresis. Lysates were diluted 10-fold in ChIP dilution buffer (20 mM Tris, 150 mM NaCl, 2 mM EDTA, and 1% Triton X-100, pH 8), and 1% was kept as the input samples. Lysates were precleared with salmon sperm DNA–blocked protein G agarose (Millipore) and incubated with 4 µg rabbit anti–Oct-1 overnight at 4°C and with protein G agarose for 2 h at 4°C. Precipitated samples were washed once with low salt washing buffer (20 mM Tris, 50 mM NaCl, 2 mM EDTA, 0.1% SDS, and 1% Triton X-100, pH 8), once with high salt washing buffer (low salt buffer with 500 mM NaCl), twice with lithium chloride washing buffer (10 mM Tris, 250 mM lithium chloride, 1 mM EDTA, 0.5% NP-40, and 0.5% SDS, pH 8), and twice with Tris EDTA buffer (10 mM Tris, pH 7.5, and 1 mM EDTA). Protein–DNA complexes were eluted using 0.1 mM $NaHCO_3$ and 1% SDS (which was also added to the input samples), and cross-links were reversed by heating overnight at 65°C. Samples were treated with 40 µg/ml proteinase K, and DNA was recovered by phenol/chloroform extraction and ethanol precipitation. All immunoprecipitated DNA samples were resuspended in 50 µl of 10 mM Tris-HCl, pH 8.5.

qRT-PCR of immunoprecipitated DNA

qRT-PCR was performed using a Rotor-Gene 3000 (Corbett Research) and the MESA GREEN qPCR MasterMix Plus for SYBR Assay (Eurogentec). PCR mixtures contained 2 µl immunoprecipitate or input samples and a final primer concentration of 400 nM. Relative gene expression values were determined using the $2^{-\Delta\Delta Ct}$ method (Livak and Schmittgen, 2001). The C_t values from qRT-PCR were normalized using those of the input samples and were used to calculate the fold enrichment of Oct-1 binding in *Lmnb1*$^{\Delta/\Delta}$ cells compared with WT cells.

Primer and oligonucleotide design

Promoter sequences (1,000 bases) of *Rdm1*, *Gpx3*, *Mmp13*, *Mgst1*, and *Serping1* were obtained using BioMart. MAPPER (Marinescu et al., 2005) was used to identify potential Oct-1–binding sites within these sequences, and appropriate primers for qRT-PCR were designed using Oligo Perfect Designer (Invitrogen). Primers for the detection of *Csnb* and *Actb* have been described previously (Zhao et al., 2004; Dong and Zhao, 2007). FAM-labeled oligonucleotides and complementary oligonucleotides corresponding to the potential Oct-1–binding sites were synthesized by Invitrogen. The oligonucleotides were annealed in 20 mM Tris-HCl, pH 8, 50 mM NaCl, and 1 mM EDTA by heating to 95°C for 5 min and gradually reducing the temperature (0.5°C/s) to 22°C. The Oct-1 consensus oligonucleotide and the sequences of all other predicted Oct-1–binding sites are provided in Table S1 (available at http://www.jcb.org/cgi/content/full/jcb.200804155/DC1).

EMSA

Approximately 10^7 cells were allowed to swell in 10 mM Hepes, pH 7.9, 1.5 mM $MgCl_2$, 10 mM KCl, 1 mM DTT, and 0.5 mM PMSF and left on ice for 10 min. NP-40 was added to a final concentration of 0.3%, and the lysates were left on ice for a further 20 min. After centrifugation, the resulting pellet was resuspended in 20 mM Hepes, pH 7.9, 25% glycerol, 0.42 M NaCl, 1.5 mM $MgCl_2$, 1 mM DTT, and 1 mM PMSF, incubated at 4°C with constant agitation, and centrifuged at 16,000 *g* for 20 min, and the supernatants (nuclear extracts) were used for the gel shift assays. Equal amounts of nuclear extracts (15 µg) were incubated with FAM-labeled oligonucleotides and excess, unlabeled Oct-1 consensus oligonucleotides in EMSA-binding buffer where applicable (final concentrations of 10 mM Tris-HCl, pH 7.5, 10% glycerol, 50 mM KCl, 1 mM $MgCl_2$, 0.5 mM DTT, and 0.5 mM PMSF) for 40 min at 22°C. Reaction mixtures were run on 8% nondenaturing polyacrylamide gels in 0.5× Tris-borate-EDTA, and the gels were photographed using an imaging system (VersaDoc MP3000; Bio-Rad Laboratories).

Online supplemental material

Fig. S1 shows lamin B1–Oct-1 colocalization using antibodies, Fig. S2 shows more extensive EMSA data, Fig. S3 shows calculated probability distribution for two microarray datasets having *n* genes in common, and Fig. S4 shows the Oct-1–binding sequence patterns identified by the MAPPER algorithm. In addition, Table S1 shows the oligonucleotide sequences used in the EMSA experiments, and Table S2 lists the genes that are dysregulated in both datasets. Online supplemental material is available at http://www.jcb.org/cgi/content/full/jcb.200804155/DC1.

We wish to record our gratitude to Stephen Young and Martin Bergo for providing both the WT and lamin B1 hypomorph transgenic mouse embryonic fibroblasts used in this study and in previous studies (Maske et al., 2003; Malhas et al., 2007), to Dr. S. Murphy for providing the Oct-1–EGFP construct, and to Professor D. Tantin for providing the WT and *Oct1*$^{-/-}$ cells. We wish to acknowledge the BioImaging Facility (Sir William Dunn School of Pathology) and the Computational Biology Research Group (Medical Sciences Division at the University of Oxford) for use of their services in this project.

This work was funded by grants from the Edward Penley Abraham Trust and by Tim and Kit Kemp. A.N. Malhas is a Kemp Postdoctoral Fellow of Lincoln College at the University of Oxford.

Submitted: 28 April 2008
Accepted: 11 December 2008

References

Ali, S.S., C. Xiong, J. Lucero, M.M. Behrens, L.L. Dugan, and K.L. Quick. 2006. Gender differences in free radical homeostasis during aging: shorter-lived female C57BL6 mice have increased oxidative stress. *Aging Cell.* 5:565–574.

Aydemir, B., I. Onaran, A.R. Kiziler, B. Alici, and M.C. Akyolcu. 2007. Increased oxidative damage of sperm and seminal plasma in men with idiopathic infertility is higher in patients with glutathione S-transferase Mu-1 null genotype. *Asian J. Androl.* 9:108–115.

Baldi, P., and A.D. Long. 2001. A Bayesian framework for the analysis of microarray expression data: regularized t-test and statistical inferences of gene changes. *Bioinformatics.* 17:509–519.

Botquin, V., H. Hess, G. Fuhrmann, C. Anastassiadis, M.K. Gross, G. Vriend, and H.R. Scholer. 1998. New POU dimer configuration mediates antagonistic control of an osteopontin preimplantation enhancer by Oct-4 and Sox-2. *Genes Dev.* 12:2073–2090.

Capanni, C., E. Mattioli, M. Columbaro, E. Lucarelli, V.K. Parnaik, G. Novelli, M. Wehnert, V. Cenni, N.M. Maraldi, S. Squarzoni, and G. Lattanzi. 2005. Altered pre-lamin A processing is a common mechanism leading to lipodystrophy. *Hum. Mol. Genet.* 14:1489–1502.

Cheng, C.K., C.M. Yeung, R.L. Hoo, B.K. Chow, and P.C. Leung. 2002. Oct-1 is involved in the transcriptional repression of the gonadotropin-releasing hormone receptor gene. *Endocrinology.* 143:4693–4701.

Choe, S.E., M. Boutros, A.M. Michelson, G.M. Church, and M.S. Halfon. 2005. Preferred analysis methods for Affymetrix GeneChips revealed by a wholly defined control dataset. *Genome Biol.* 6:R16.

Chuang, C.H., A.E. Carpenter, B. Fuchsova, T. Johnson, P. de Lanerolle, and A.S. Belmont. 2006. Long-range directional movement of an interphase chromosome site. *Curr. Biol.* 16:825–831.

dela Paz, N.G., S. Simeonidis, C. Leo, D.W. Rose, and T. Collins. 2007. Regulation of NF-kappaB-dependent gene expression by the POU domain transcription factor Oct-1. *J. Biol. Chem.* 282:8424–8434.

Dong, B., and F.Q. Zhao. 2007. Involvement of the ubiquitous Oct-1 transcription factor in hormonal induction of beta-casein gene expression. *Biochem. J.* 401:57–64.

Dreuillet, C., J. Tillit, M. Kress, and M. Ernoult-Lange. 2002. In vivo and in vitro interaction between human transcription factor MOK2 and nuclear lamin A/C. *Nucleic Acids Res.* 30:4634–4642.

Dreuillet, C., M. Harper, J. Tillit, M. Kress, and M. Ernoult-Lange. 2008. Mislocalization of human transcription factor MOK2 in the presence of pathogenic mutations of lamin A/C. *Biol. Cell.* 100:51–61.

Eriksson, M., W.T. Brown, L.B. Gordon, M.W. Glynn, J. Singer, L. Scott, M.R. Erdos, C.M. Robbins, T.Y. Moses, P. Berglund, et al. 2003. Recurrent de novo point mutations in lamin A cause Hutchinson-Gilford progeria syndrome. *Nature.* 423:293–298.

Finkel, T., and N.J. Holbrook. 2000. Oxidants, oxidative stress and the biology of ageing. *Nature.* 408:239–247.

Fu, Y., J.M. Porres, and X.G. Lei. 2001. Comparative impacts of glutathione peroxidase-1 gene knockout on oxidative stress induced by reactive oxygen and nitrogen species in mouse hepatocytes. *Biochem. J.* 359:687–695.

Glynn, M.W., and T.W. Glover. 2005. Incomplete processing of mutant lamin A in Hutchinson-Gilford progeria leads to nuclear abnormalities, which are reversed by farnesyltransferase inhibition. *Hum. Mol. Genet.* 14:2959–2969.

Goldman, R.D., Y. Gruenbaum, R.D. Moir, D.K. Shumaker, and T.P. Spann. 2002. Nuclear lamins: building blocks of nuclear architecture. *Genes Dev.* 16:533–547.

Guelen, L., L. Pagie, E. Brasset, W. Meuleman, M.B. Faza, W. Talhout, B.H. Eussen, A. de Klein, L. Wessels, W. de Laat, and B. van Steensel. 2008.

Downloaded from http://rupress.org/jcb/article-pdf/184/1/45/1555786/jcb_200804155.pdf by guest on 08 February 2026

Domain organization of human chromosomes revealed by mapping of nuclear lamina interactions. *Nature.* 453:948–951.

Haithcock, E., Y. Dayani, E. Neufeld, A.J. Zahand, N. Feinstein, A. Mattout, Y. Gruenbaum, and J. Liu. 2005. Age-related changes of nuclear architecture in *Caenorhabditis elegans*. *Proc. Natl. Acad. Sci. USA.* 102:16690–16695.

Hayes, J.D., and R.C. Strange. 2000. Glutathione S-transferase polymorphisms and their biological consequences. *Pharmacology.* 61:154–166.

Heessen, S., and M. Fornerod. 2007. The inner nuclear envelope as a transcription factor resting place. *EMBO Rep.* 8:914–919.

Hewitt, S.L., F.A. High, S.L. Reiner, A.G. Fisher, and M. Merkenschlager. 2004. Nuclear repositioning marks the selective exclusion of lineage-inappropriate transcription factor loci during T helper cell differentiation. *Eur. J. Immunol.* 34:3604–3613.

Imai, S., S. Nishibayashi, K. Takao, M. Tomifuji, T. Fujino, M. Hasegawa, and T. Takano. 1997. Dissociation of Oct-1 from the nuclear peripheral structure induces the cellular aging-associated collagenase gene expression. *Mol. Biol. Cell.* 8:2407–2419.

Ivorra, C., M. Kubicek, J.M. Gonzalez, S.M. Sanz-Gonzalez, A. Alvarez-Barrientos, J.E. O'Connor, B. Burke, and V. Andres. 2006. A mechanism of AP-1 suppression through interaction of c-Fos with lamin A/C. *Genes Dev.* 20:307–320.

Kenworthy, A.K. 2001. Imaging protein-protein interactions using fluorescence resonance energy transfer microscopy. *Methods.* 24:289–296.

Kim, M.K., L.A. Lesoon-Wood, B.D. Weintraub, and J.H. Chung. 1996. A soluble transcription factor, Oct-1, is also found in the insoluble nuclear matrix and possesses silencing activity in its alanine-rich domain. *Mol. Cell. Biol.* 16:4366–4377.

Lans, H., and J.H. Hoeijmakers. 2006. Cell biology: ageing nucleus gets out of shape. *Nature.* 440:32–34.

Livak, K.J., and T.D. Schmittgen. 2001. Analysis of relative gene expression data using real-time quantitative PCR and the 2(-Delta Delta C(T)) Method. *Methods.* 25:402–408.

Lloyd, D.J., R.C. Trembath, and S. Shackleton. 2002. A novel interaction between lamin A and SREBP1: implications for partial lipodystrophy and other laminopathies. *Hum. Mol. Genet.* 11:769–777.

Malhas, A., C.F. Lee, R. Sanders, N.J. Saunders, and D.J. Vaux. 2007. Defects in lamin B1 expression or processing affect interphase chromosome position and gene expression. *J. Cell Biol.* 176:593–603.

Marinescu, V.D., I.S. Kohane, and A. Riva. 2005. MAPPER: a search engine for the computational identification of putative transcription factor binding sites in multiple genomes. *BMC Bioinformatics.* 6:79.

Maske, C.P., M.S. Hollinshead, N.C. Higbee, M.O. Bergo, S.G. Young, and D.J. Vaux. 2003. A carboxyl-terminal interaction of lamin B1 is dependent on the CAAX endoprotease Rce1 and carboxymethylation. *J. Cell Biol.* 162:1223–1232.

Orosz, Z., A. Csiszar, N. Labinskyy, K. Smith, P.M. Kaminski, P. Ferdinandy, M.S. Wolin, A. Rivera, and Z. Ungvari. 2007. Cigarette smoke-induced proinflammatory alterations in the endothelial phenotype: role of NAD(P)H oxidase activation. *Am. J. Physiol. Heart Circ. Physiol.* 292:H130–H139.

Otto, H., M. Dreger, L. Bengtsson, and F. Hucho. 2001. Identification of tyrosine-phosphorylated proteins associated with the nuclear envelope. *Eur. J. Biochem.* 268:420–428.

Ouyang, X., T.L. DeWeese, W.G. Nelson, and C. Abate-Shen. 2005. Loss-of-function of Nkx3.1 promotes increased oxidative damage in prostate carcinogenesis. *Cancer Res.* 65:6773–6779.

Remenyi, A., A. Tomilin, H.R. Scholer, and M. Wilmanns. 2002. Differential activity by DNA-induced quarternary structures of POU transcription factors. *Biochem. Pharmacol.* 64:979–984.

Rozet, J.M., S. Gerber, I. Perrault, P. Calvas, E. Souied, S. Chatelin, P. Viegas, D. Molina-Gomez, A. Munnich, and J. Kaplan. 1998. Structure and refinement of the physical mapping of the gamma- glutamylcysteine ligase regulatory subunit (GLCLR) gene to chromosome 1p22.1 within the critically deleted region of human malignant mesothelioma. *Cytogenet. Cell Genet.* 82:91–94.

Saal, L.H., C. Troein, J. Vallon-Christersson, S. Gruvberger, A. Borg, and C. Peterson. 2002. BioArray Software Environment (BASE): a platform for comprehensive management and analysis of microarray data. *Genome Biol.* 3:SOFTWARE0003.

Sanchez Ferrer, A., J.S. Santema, R. Hilhorst, and A.J. Visser. 1990. Fluorescence detection of enzymatically formed hydrogen peroxide in aqueous solution and in reversed micelles. *Anal. Biochem.* 187:129–132.

Sanchez-Font, M.F., J. Sebastia, C. Sanfeliu, R. Cristofol, G. Marfany, and R. Gonzalez-Duarte. 2003. Peroxiredoxin 2 (PRDX2), an antioxidant enzyme, is under-expressed in Down syndrome fetal brains. *Cell. Mol. Life Sci.* 60:1513–1523.

Scaffidi, P., and T. Misteli. 2006. Lamin A-dependent nuclear defects in human aging. *Science.* 312:1059–1063.

Steinbrenner, H., L. Alili, E. Bilgic, H. Sies, and P. Brenneisen. 2006. Involvement of selenoprotein P in protection of human astrocytes from oxidative damage. *Free Radic. Biol. Med.* 40:1513–1523.

Tang, C.W., A. Maya-Mendoza, C. Martin, K. Zeng, S. Chen, D. Feret, S.A. Wilson, and D.A. Jackson. 2008. The integrity of a lamin-B1-dependent nucleoskeleton is a fundamental determinant of RNA synthesis in human cells. *J. Cell Sci.* 121:1014–1024.

Tantin, D., C. Schild-Poulter, V. Wang, R.J. Hache, and P.A. Sharp. 2005. The octamer binding transcription factor Oct-1 is a stress sensor. *Cancer Res.* 65:10750–10758.

Toth, J.I., S.H. Yang, X. Qiao, A.P. Beigneux, M.H. Gelb, C.L. Moulson, J.H. Miner, S.G. Young, and L.G. Fong. 2005. Blocking protein farnesyltransferase improves nuclear shape in fibroblasts from humans with progeroid syndromes. *Proc. Natl. Acad. Sci. USA.* 102:12873–12878.

Tusher, V.G., R. Tibshirani, and G. Chu. 2001. Significance analysis of microarrays applied to the ionizing radiation response. *Proc. Natl. Acad. Sci. USA.* 98:5116–5121.

Valverde, P. 2005. Effects of Gas6 and hydrogen peroxide in Axl ubiquitination and downregulation. *Biochem. Biophys. Res. Commun.* 333:180–185.

Vergnes, L., M. Peterfy, M.O. Bergo, S.G. Young, and K. Reue. 2004. Lamin B1 is required for mouse development and nuclear integrity. *Proc. Natl. Acad. Sci. USA.* 101:10428–10433.

Wilson, K.L. 2005. Integrity matters: linking nuclear architecture to lifespan. *Proc. Natl. Acad. Sci. USA.* 102:18767–18768.

Winokur, S.T., K. Barrett, J.H. Martin, J.R. Forrester, M. Simon, R. Tawil, S.A. Chung, P.S. Masny, and D.A. Figlewicz. 2003. Facioscapulohumeral muscular dystrophy (FSHD) myoblasts demonstrate increased susceptibility to oxidative stress. *Neuromuscul. Disord.* 13:322–333.

Worman, H.J., and J.C. Courvalin. 2005. Nuclear envelope, nuclear lamina, and inherited disease. *Int. Rev. Cytol.* 246:231–279.

Wouters, F.S., and P.I. Bastiaens. 1999. Fluorescence lifetime imaging of receptor tyrosine kinase activity in cells. *Curr. Biol.* 9:1127–1130.

Yang, S.H., M. Meta, X. Qiao, D. Frost, J. Bauch, C. Coffinier, S. Majumdar, M.O. Bergo, S.G. Young, and L.G. Fong. 2006. A farnesyltransferase inhibitor improves disease phenotypes in mice with a Hutchinson-Gilford progeria syndrome mutation. *J. Clin. Invest.* 116:2115–2121.

Zhao, F.Q., Y. Zheng, B. Dong, and T. Oka. 2004. Cloning, genomic organization, expression, and effect on beta-casein promoter activity of a novel isoform of the mouse Oct-1 transcription factor. *Gene.* 326:175–187.

Zink, D., M.D. Amaral, A. Englmann, S. Lang, L.A. Clarke, C. Rudolph, F. Alt, K. Luther, C. Braz, N. Sadoni, et al. 2004. Transcription-dependent spatial arrangements of CFTR and adjacent genes in human cell nuclei. *J. Cell Biol.* 166:815–825.

Downloaded from http://rupress.org/jcb/article-pdf/184/1/45/1555786/jcb_200804155.pdf by guest on 08 February 2026